Available online at www.eccomasproceedia.org
Eccomas Proceedia SMART (2023) 269-280

ECCOMAS
Proceedia

X ECCOMAS Thematic Conference on Smart Structures and Materials
SMART 2023
D.A. Saravanos, A. Benjeddou, N. Chrysochoidis and T. Theodosiou (Eds)

SELF-CONTAINED VELOCITY FEEDBACK UNIT WITH A SEISMIC FLYWHEEL ELECTROMAGNETIC ACTUATOR

ALEKSANDER KRAS* **AND PAOLO GARDONIO †**

*Silencions
Bierutowska 57-59, 51-317 Wrocław, (PL)
e-mail: aleksander@silencions.com, www.silencions.com

†Università degli Studi di Udine - DPIA,
Via delle Scienze 206 - 33100, Udine, (IT)
email: paolo.gardonio@ uniud.it, www.uniud.it

Abstract. This paper presents a comprehensive experimental study on the working principle and the stability and performance analyses of a self-contained velocity feedback control unit, which can be used in batches to control the flexural vibration of complex-wall structures such as the fuselage of an aircraft. The control unit is formed by a seismic flywheel electromagnetic actuator with an accelerometer sensor placed at the its footprint, which are used to implement a sky-hook velocity feedback loop. The actuator is formed by an outer ferromagnetic hollowed cylinder yoke with a double coil winded on the interior rim, which is connected to an inner cylindrical magnet post via helical springs. A flywheel is mounted using torsional springs to the yoke and is connected via an eccentric pin to the inner magnet such that the linear relative oscillations of the yoke-magnet assembly generate rotational oscillations of the flywheel. This augments the seismic inertial effect such that a larger sky-hook force is generated for a given total mass of the actuator. The paper first describes in details the working principle of the seismic flywheel electromagnetic actuator. Then, it provides a comprehensive stability analysis based on the Bode and Nyquist plots of the open loop frequency response function of the control unit. Finally, it presents a case study where the actuator is mounted on thin plate to control the flexural vibrations in the low to mid frequency range where the response is characterised by distinct or clusters of resonances. The study shows that the flywheel inertial element effectively increases the stability and control performance of the velocity feedback unit, without compromising its robustness to shocks or high accelerations of the hosting structure.

Key words: Inertial actuator, proof mass actuator, velocity feedback, inerter, flywheel.

1 INTRODUCTION

This paper presents an experimental study focussed on the implementation of stable and rebuts velocity feedback loops to control flexural vibration in thin structures with the flywheel inertial actuator that was introduced in ref. [1,2]. This paper presents the measured frequency responses functions that characterise the electromechanical response, stability and control

Peer-review under responsibility of the organizing committee of SMART 2023.
doi: 10.7712/150123.9784.444256

performance of the velocity feedback loops using the flywheel inertial actuator, which are also contrasted with simulations obtained from a lumped parameter models presented in refs. [1,2].

Inertial actuators, also commonly known as proof mass actuators or reaction mass actuators, can be used to implement negative velocity feedback control loops for vibration control of thin panels and shells [3-9]. The classical inertial actuator considered in this study is built with a round magnetic element placed within a cylindrical iron armature that hosts the coil winding. These two components are connected to each other via two flexural spring. This inertial actuator is used with the heavier coil armature acting as suspended inertial mass and the lighter magnet element that acts as a base mass. When current flows through the coil placed in the magnetic field crated by the inner magnet and closed by the back iron armature, a reactive force effect is produced between the coil armature and the magnet element [10,11]. At frequencies below the fundamental resonance frequency of the actuator, the net force produced at the base of the actuator is proportional to the driving current, while at higher frequencies it is constant and in phase with the driving current [12]. Thus, when this actuator is used to implement a negative velocity feedback to act as a sky-hook damper, at frequencies below the fundamental resonance frequency, the feedback loop produces a positive velocity feedback effect that is a negative damping effect, which leads to instability. It is therefore vitally important the fundamental resonance frequency of the actuator is as low as possible and the amplitude of the resonance peak is also the minimum possible [13]. However, this solution tends to increase the static displacement of the inertial mass, which, in presence of shocks, may hit the actuator stop ends and trigger instability effects [14]. Thus, one of the key parameters that characterises the inertial actuators for vibration control with negative velocity feedback control is the static deflection that defines the robustness and ability to withstand shocks and high accelerations of the hosting structure [15,16]. The general requirements for the inertial actuators used in the velocity feedback loops are contradictory. The actuator should have low fundamental resonance frequency to produce positive damping effect in the wide frequency range but at the same time it should have low static deflection to be more robust to shocks of the hosting structure [17-19]. Thus, the classical inertial actuators are more exposed to shocks, which can cause the proof mass to hit the end stops and induce instability of the velocity feedback loops.

The prototype presented in this study is based on the classical actuator with an additional flywheel element that is used to augment the inertia effect of the inertial mass [20,21]. The flywheel inertial actuator, presented in this paper, uses the axial inertia effect of the flywheel to reduce the fundamental resonance frequency of the inertial actuator without increasing the static deflection of the springs-proof mass assembly. The experimental and theoretical investigation presented in this study shows advantages of the flywheel inertial actuator.

2 ACTUATORS DESCRIPTION AND CONFIGURATIONS

The classical inertial actuator used for vibration control application considered in this study is based on a coil–magnet linear transducer shown in Figure 1a, which has been studied with the lumped elements model shown in the right graph of Figure 1a. The detail of the mathematical model are given in refs. [1,2]. The transducer is built with an inner round permanent magnet that acts as a base mass m_b and an outer cylindrical armature that acts as a proof mass M_a where

the coil is housed. The external coil armature is connected to the inner magnetic element via two flexural springs of stiffness k, which are also used to suspend the inertial mass. The damping effect c is created by the small air gap between coil and magnet and by the eddy currents generated in the laminated plates of the coil armature. The electro-magnetic effect that produces a pair of reactive forces F_a between the base mass (magnet) and inertial mass (coil armature) is modelled in terms of transduction coefficient ψ_a and the current i_a flowing in the coil. The voltage u_a applied at the electrical terminals of the actuator is proportional to the coil resistance R and inductance L. The back electromotive force u_{em} is generated by the relative motion of the coil placed in the magnetic field and is proportional to the relative velocity between the proof mass and the base mass.

To obtain the best similarity to the fabricated flywheel prototypes the classical configuration presented in this study was based on the flywheel inertial actuator. The flywheel element and its supporting bracket was attached to the external coil armature, while the base linking pin was disconnected to deactivate the axial inertia effect produced by the flywheel element as shown in the picture of Figure 1a. Thus, the classical configuration presented in this study is characterised by the equal inertial mass as the proposed flywheel prototypes, where the inertial mass equals sum of the proof mass M_a and flywheel mass m_w, as shows with the lumped elements model in Figure 1a.

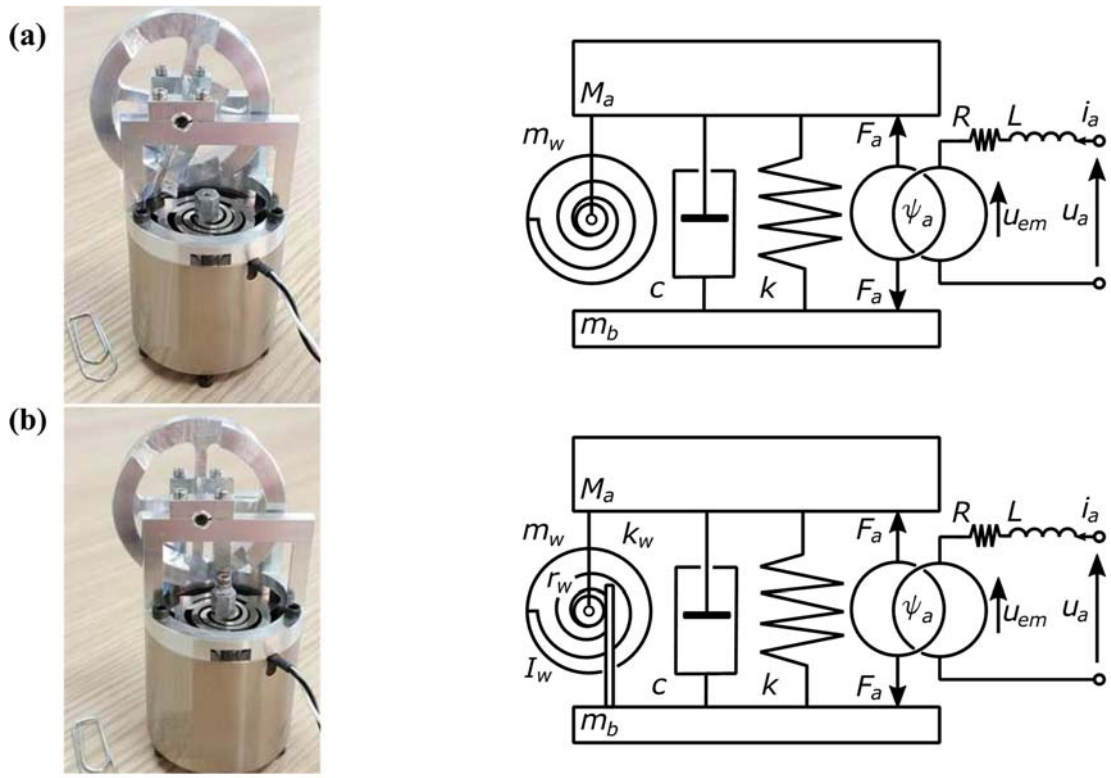

Figure 1: Schemes and pictures of the tested classical (a) and the flywheel (b) inertial actuators.

The flywheel proof mass actuator shown in Figure 1b with lumped elements model shown in the right graph was equipped with the flywheel element. The additional flywheel element was designed in the form of a round wheel with polar moment of inertia I_w and mass m_w. The flywheel element was designed in several configurations having the same mass with different polar moment of inertia values so thus it could produce different axial inertia effects to the inertial transducer. The flywheel element was suspended with two flexural bearings of torsional stiffness k_w. The third frictionless pivot bearing connects the flywheel element with the case of the actuator via designed pushing pin mounted with an offset r_w from the flywheel horizontal axis of rotation to produce rotational oscillations of the flywheel.

The physical properties of the classical coil-magnet actuator and the flywheel actuator are summarised in Table 1. The table specifies three values of the equivalent axial inertia I_w / (r_w^2) effect for different flywheel configurations.

Table 1: Mechanical parameters of the classical and flywheel inertial actuators.

Parameter	Value
Proof mass	$M_a = 0.185$ kg
Case mass	$m_b = 0.115$ kg
Flywheel system mass	$m_w = 0.045$ kg
Axial stiffness	$k = 2950$ Nm^{-1}
Torsional stiffness	$k_w = 0.003$ Nmrad^{-1}
Damping ratio	$\zeta = 0.2$
Pushing pin offset values	$r_w = 6.4$ mm
I Flywheel inertance	$I_{w1}/r_{w1}^2 = 0.166$ kg
II Flywheel inertance	$I_{w2}/r_{w2}^2 = 0.256$ kg
III Flywheel inertance	$I_{w3}/r_{w3}^2 = 0.353$ kg
Coil resistance	$R = 22.5\ \Omega$
Coil inductance	$L = 4.35 \cdot 10^{-3}$ H
Transduction coefficient	$\psi_a = 22.5$ NA^{-1}

3 MECHANICAL BASE IMPEDANCE

The Bode plots in Figure 2 show the base impedance FRFs of the classical and the flywheel inertial actuator. The figure is organised in two columns where, the left column shows the modulus diagrams while the right column shows the phase diagrams. The solid lines in the figure present the measurement results, while the dashed lines present the simulation results [1,2]. Plot (a) shows the base impedance of the classical proof mass actuator, while plots (b,c,d) show the base impedance of the flywheel inertial actuator with increasing value of the flywheel inertance.

The modulus of the base impedance for the classical configuration showed in left diagram of the Figure 2a is characterised by low and high frequencies asymptotic mass behaviours separated by a resonance peak and antiresonance through. The resonance peak appears at about the fundamental resonance frequency of 19 Hz while the antiresonance through at about 33 Hz. The phase of the base impedance for the classical configuration showed in right diagram of the Figure 2a is characterised by the two shifts. At the resonance peak the base impedance phase

shifts from +90° to around -10° while at the antiresonance the phase shifts back from 0° to +90°. The measured base impedance for the classical configuration agree well with the simulated values.

The base impedances for the flywheel inertial actuator shown in Figure 2b,c,d present similar characteristic to the classical configuration. However, the fundamental resonance frequency is moved to about 14 Hz in Figure 2b, to about 12 Hz in Figure 2c and to about 10 Hz in Figure 2d. Consequently, the antiresonance through is also influenced by the axial inertia effect produced by the flywheel element. The antiresonance through is moved to about 20 Hz in Figure 2b, to about 16.5 Hz in Figure 2c and to about 13.5 Hz in Figure 2d. The amplitude of the lower frequency asymptotic mass behaviour is the same as the classical inertial actuator because both configurations are characterised with the same total mass. The experimental results align well with the simulated base impedance FRFs for all configurations.

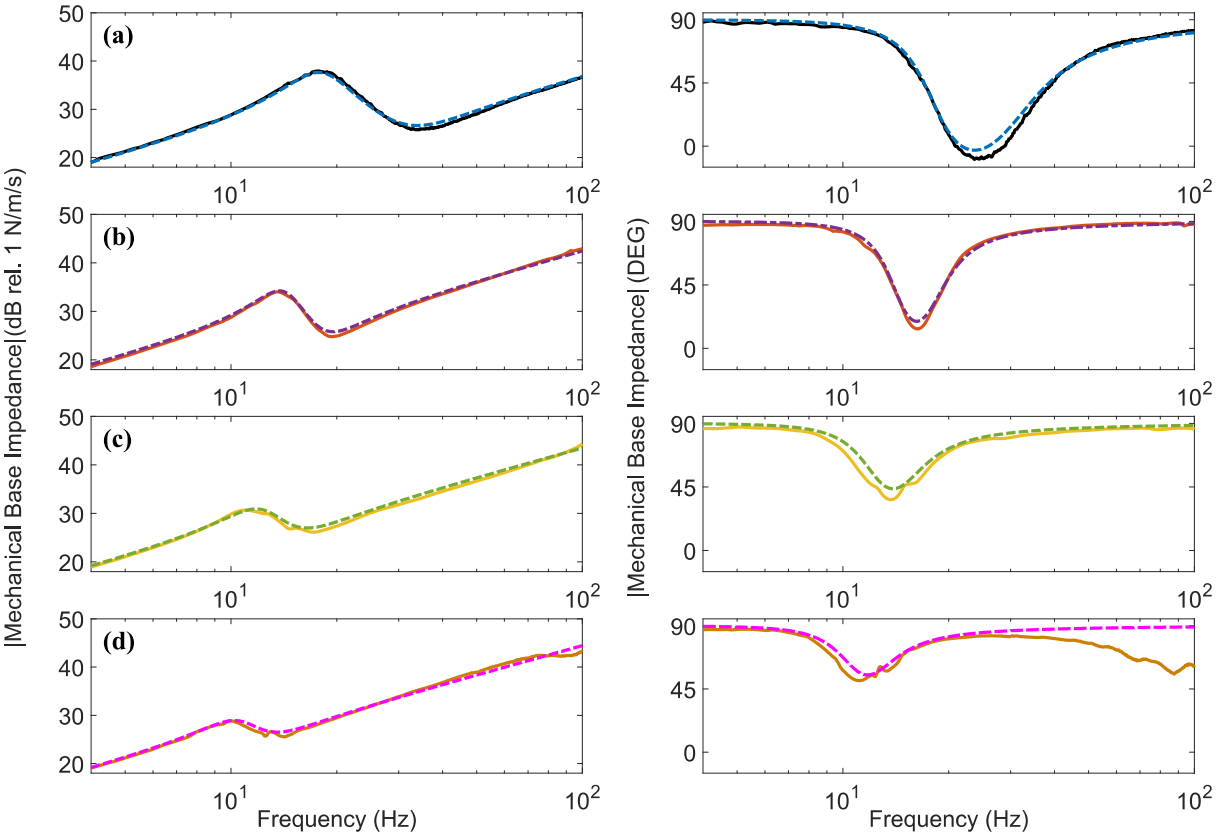

Figure 2: Actuator base impedance for the classical inertial actuator (a) and the flywheel inertial actuator with the increasing inertance I_{w1}/r_{w1}^2 (b), I_{w2}/r_{w2}^2 (c), I_{w3}/r_{w3}^2 (d) respectively to Table 1. Comparison of the experimental results (solid lines) with the numerical simulations (dashed lines).

4 IMPLEMENTATION OF THE VELOCITY FEEDBACK CONTROL LOOPS

This section presents an experimental study on the implementation of a velocity feedback loop with the classical and flywheel inertial actuators to control vibration in thin rectangular panel. The experimental test setup are used to evaluate the stability and control performance of the velocity feedback loops using the classical and the flywheel inertial actuators with inertance value of the flywheel element. The stability of the velocity feedback loops using the classical and the flywheel inertial actuators was assessed using the Nyquist criterion based on the open loop sensor – actuator FRF. The control performance has been assessed by plotting the total flexural kinetic energy of the rectangular plate.

The picture of the test setup with of the velocity feedback loop implemented on thin rectangular panel is shown in Figure 3. The tested actuators were attached on the one side of the panel, while the small accelerometer sensor used to measure the error signal was attached on the other side of the panel. The primary excitation point force produced by a shaker was located on the same side of the panel as accelerometer.

The velocity feedback control loops were implemented with an analogue conditioner that filtered and integrated the signal obtained from the accelerometer, as shown in the lumped parameter model of Fig 7b. The output velocity signal was sent back to the actuator via a voltage operational amplifier that increased the gain of the error signal. The experimental results were compared with the numerical simulations obtained from the lumped parameter model of the actuators located on the rectangular panel.

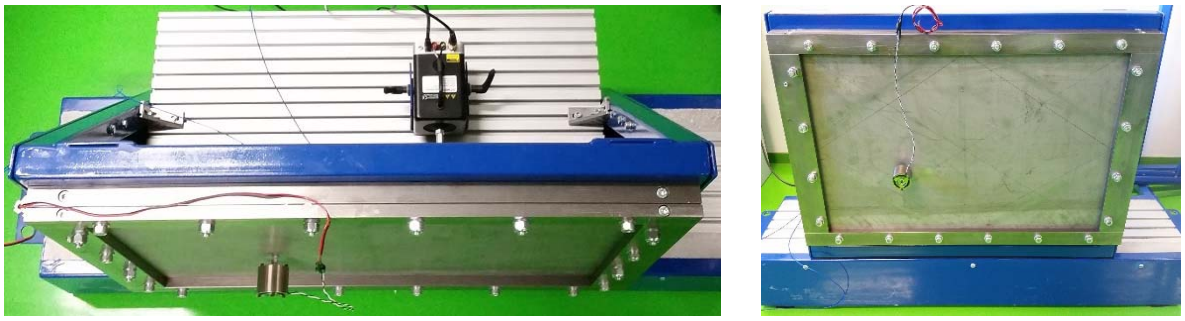

Figure 3: View from the top (left) and from the front (right) of the structure of a rectangular plate with a velocity feedback control loop system using the inertial actuator. Small shaker was used to excite the plate, while the control inertial actuator was attached on the other side to the plate.

4 STABILITY

The stability of the velocity feedback loops using the classical inertial actuator and the flywheel inertial actuators is assessed using the Nyquist criterion. Figure 4 shows the bode diagram of the open loop sensor – actuator FRF for the classical inertial actuator (Figure 4a) and flywheel inertial actuator with the third inertance value I_{w3}/r_{w3}^2 (Figure 4b). The solid lines in the plots present the measurement results, while the dashed lines present the simulation results of the open loop sensor – actuator FRF which can be found in [2].

The Bode plot of the open loop sensor – actuator FRF for the classical inertial actuator shown in Figure 4a is characterised by heavily damped resonance at about 18 Hz, which is due to the

fundamental resonance of the inertial actuator, and then a sequence of resonance peaks, which are due to due to low order natural modes of the plate. The phase plot starts at +270° at low frequency then it drops to +90° beyond the fundamental resonance frequency of the inertial actuator at about 35 Hz and then oscillates with a sequence of -180° phase lag and +180° phase lead for each resonance peak and antiresonance low pair. Also, the phase starts to slowly decade with the frequencies due to the increase of the coil electrical impedance for the voltage driven actuator.

The measured open loop sensor – actuator FRF for the classical inertial actuator presents similar characteristic to the simulation results and it aligns well at low frequency. Compared to the experimental results, the simulation results present small difference in the amplitude and frequency between 400 Hz and 600 Hz. The simulated phase of the open loop sensor–actuator FRF aligns well with the measured one.

The bode plot for the flywheel inertial actuator shown in Figure 4b is characterised by a heavily damped resonance at about 12 Hz, which is due to the fundamental resonance of the flywheel inertial actuator. The phase of the open loop sensor – actuator FRF starts at +270° at low frequency and drops to +90 at much lower frequency, of about 25 Hz compared to the classical inertial actuator. At higher frequencies, the phase oscillates with a sequence of -180° phase lag and +180° phase lead for each resonance peak and antiresonance low pair.

The measured open loop sensor – actuator FRF for the flywheel inertial actuator presents similar characteristic to the simulations and aligns well with the measured one. However, at higher frequencies, more precisely above 400 Hz, the sequence of resonance peaks and antiresonance lows pairs tends to smoothen as the frequency rises. However, the measurement results show that these resonances and antiresonances maintain rather sharp.

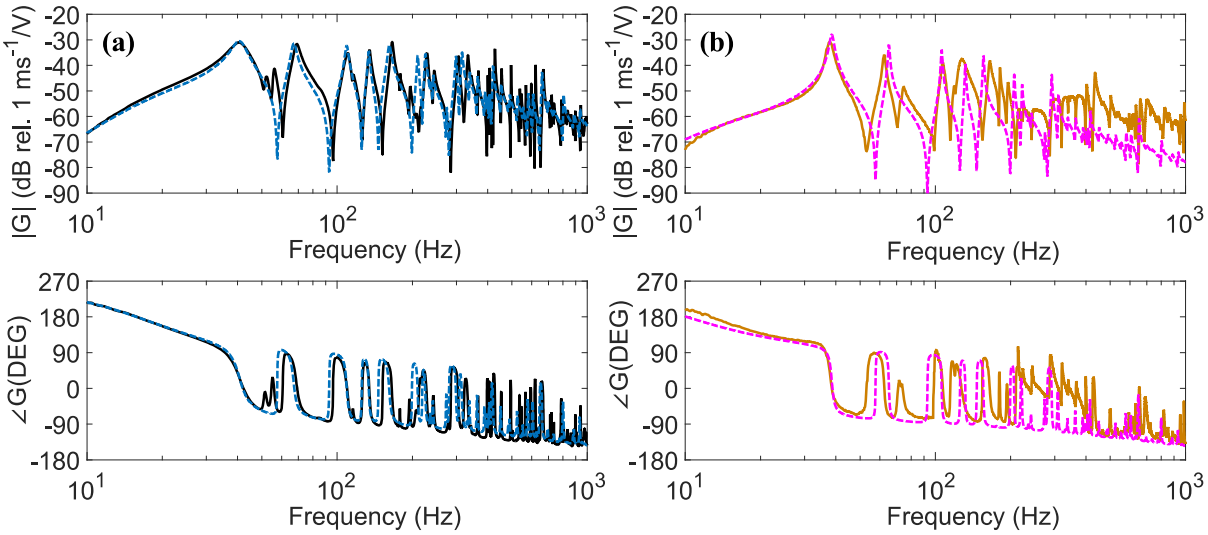

Figure 4: Bode diagram of the open loop sensor–actuator FRFs for the classical inertial actuator (a) and flywheel inertial actuator (b). Comparison of the experimental results (solid lines) with the numerical simulations (dashed lines).

The Nyquist plot for the feedback loop with the classical inertial actuator shown in Figure 5a confirms the analysis presented with the bode plot shown in Figure 4a. The Nyquist diagram is characterised by a circle in the real negative quadrants, which is due to the heavily damped resonance of the actuator, and then a series of circles in the real positive quadrants, which are due to the resonances of the plate. The circle on the real negative quadrants indicates that the control system is found to be only conditionally stable. Thus, the maximum stable signal gain margin for the classical inertial actuator is about 55 dB.

The Nyquist diagram for flywheel inertial actuator shown in Figure 5b presents similar characteristics to the Nyquist plot of the open loop sensor – actuator FRF for the classical inertial actuator and confirms the analysis presented with the bode plot shown in Figure 4b. The diagram is characterised by a circle in the real negative quadrants, which is due to fundamental resonance frequency of the flywheel actuator, and then a series of circles in the real positive quadrants, which are due to the resonances of the plate. The control system for the flywheel inertial actuator is also conditionally stable, with the maximum stable signal gain margin equal to about 68 dB, which is 13 dB higher compared to the velocity feedback loops with classical inertial actuator.

This phase shift shown in the Bode plots in Figure 4 is also seen in the Nyquist plots and is characterised by a circle in the real negative quadrants. The circle due to the additional dynamics does not interfere the stability of the feedback loops defined by the larger semicircle which is due to fundamental resonance frequency of the actuator.

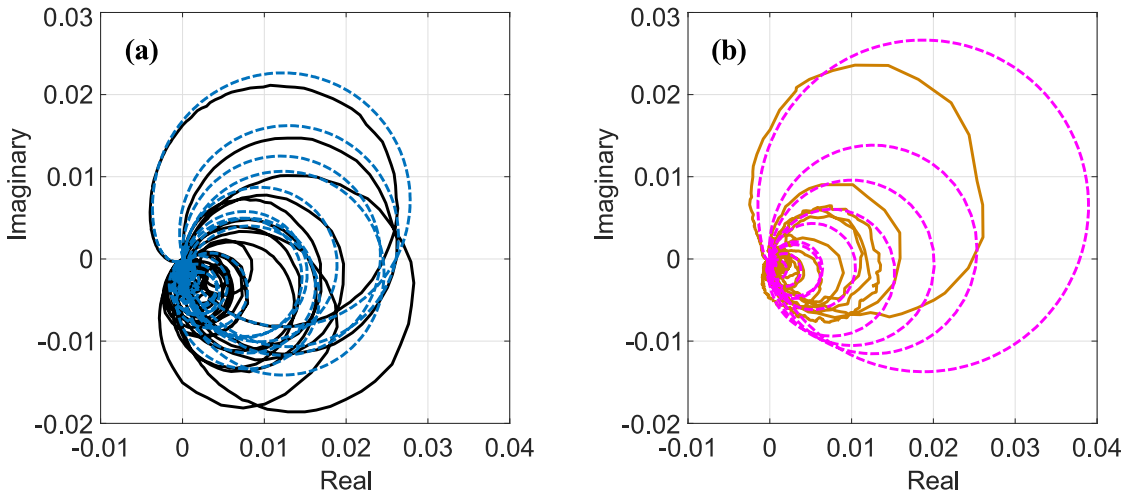

Figure 5: Nyquist plots of the open loop sensor–actuator FRFs for the classical (a) and flywheel inertial actuator with third axial inertia effect (b). Comparison of the experimental results (solid lines) with the numerical simulations (dashed red lines).

5 PERFORMANCE

The performance of the velocity feedback loops with the classical and the flywheel inertial actuators is also assessed considering the total flexural kinetic energy of the rectangular plate. The plots in Figure 6 show the total flexural kinetic energy of the rectangular plate per unit

force of excitation for the plate without actuators (dotted red lines), the plate equipped with the feedback loop with maximum signal gain that guarantee stability applied to the inertial actuators, for the classical inertial actuator (blue and black lines), and the flywheel inertial actuators with third I_{w3}/r_{w3}^2 (magenta and brown lines) axial inertia effect. Figure 6a show the simulation results while the Figure 6b show the measurement results.

The kinetic energy spectrum of the plane plate without any inertial actuator (dotted red lines) is characterised by fundamental resonance peak at about 43 Hz and then a sequence of progressively smaller in amplitude sharp resonance peaks. The numerical results for the plain plate shown in Figure 6a correspond quite well to the experimental results shown Figure 6b.

Considering the kinetic energy of the plate when the velocity feedback loops are implemented with maximum control gains that ensure stability using the inertial actuators the spectra are characterised by rounded off plate resonance peaks. Results show that the velocity feedback loops with the maximum control gains produce similar reductions of the plate fundamental resonance peak. However, the spectra also show that the velocity feedback loops generate high control spillover effects around the fundamental resonance frequency of the actuators. The plots in Figure 6b clearly show that the feedback loop with the classical proof mass actuator generates at the fundamental resonance frequency of the actuator, at about 18 Hz, a high control spillover effect, which has amplitude of about -68 dB. The feedback loops using the flywheel inertial actuator with the third I_{w3}/r_{w3}^2 axial inertia effect generates the smallest control spillover at even lower frequency of about 12 Hz that has amplitude of about -100 dB.

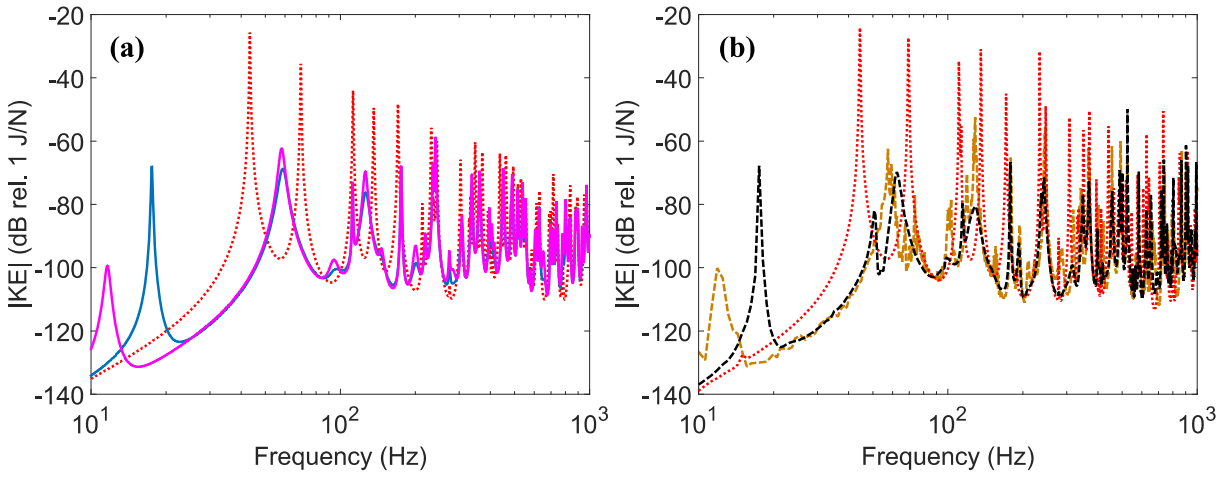

Figure 6: Simulated (a) and measured (b) total flexural kinetic energy per unit force excitation of the plate without proof mass actuator (dotted red lines) and for the plate with control feedback loops with maximum signal gain that guarantee stability applied to classical inertial actuator (blue and black lines) and the flywheel inertial actuator (magenta and brown lines).

Thus, the kinetic energy spectra show that when the feedback loop with the flywheel configurations are implemented the spillover effects have lower amplitude by about 32 dB of the flywheel prototype compared to the classical inertial actuator. This is principally due to reduced fundamental resonance frequency of the flywheel actuator that improved stability and

performance of the velocity feedback loops.

Comparing numerical and measurement results it can observed that at low frequencies the performance of the velocity feedback loops can be predicted quite precisely for flywheel inertial actuator. Although, the results for the third configuration of the flywheel inertial actuator presented with dashed brown line present slight noise, the numerical results presented with solid magenta line correspond well with the experimental results.

To better asses the effectiveness of the proposed control systems, the 10 Hz to 1 kHz frequency averaged plate kinetic energy reduction is considered with reference to feedback control gains signal applied the inertial actuator. The reductions of the frequency averaged flexural kinetic energy of the plate equipped with the feedback control units are normalised with reference to the frequency averaged kinetic energy of the plain plate without any inertial actuator. Figure 7 shows reduction of the frequency average kinetic energy when the feedback loops are implemented using the classical inertial actuator (solid black line) and the flywheel configuration (dashed brown line). The results show the frequency averaged plate kinetic energy reduction with increasing feedback control signals up to maximum (square marker) control gain that guarantees stability. Figure 7 also shows points (circle marker) with performance for the 10 dB signal margin that should be used in practical applications to improve stability and robustness of the velocity feedback loops in case of shocks of the hosting structure.

Figure 7 shows that when the feedback loops are implemented using the classical inertial actuator the maximum kinetic energy reduction is about 15.5 dB (black square). Instead when the feedback loops are implemented using the flywheel inertial actuator the maximum kinetic energy reduction is about 16.2 dB.

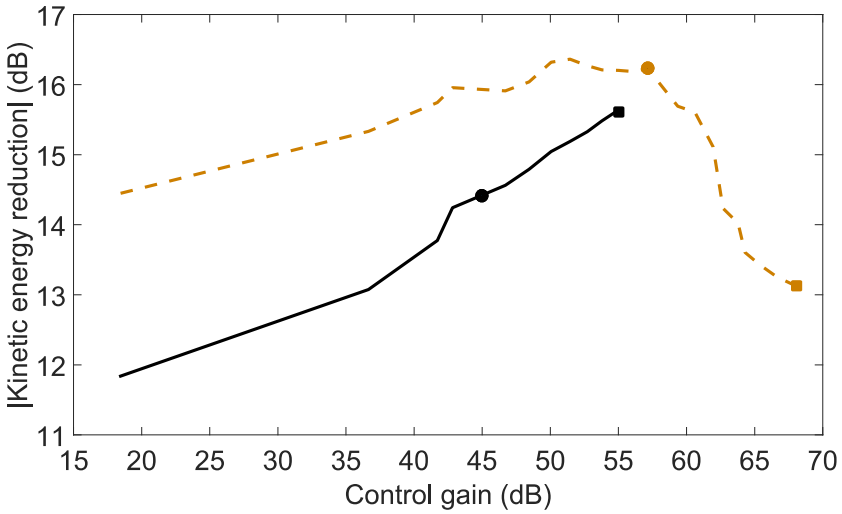

Figure 7: Frequency averaged total flexural kinetic energy for the increasing value of the feedback control signal gain applied to the classical inertial actuator (solid black line) and to the flywheel inertial actuator with the third I_{w3}/r_{w3}^2 (dashed brown line) axial inertia effect. The dot markers present the results for the 10 dB signal gain margin, while the square markers present the results for the maximum stable signal gain.

The frequency averaged plate kinetic energy reduction also shows that although the velocity feedback loops with the flywheel inertial actuator (dashed brown line) configuration of the flywheel element allows to implement rather high signal gains, which tends to drop the overall performance of the control system. This performance drop is related to the pinning effect generated by the inertial actuator, which is creating a new boundary condition of the plate and instead of reducing vibrations it modifies the rectangular plate response. Nevertheless, when the feedback loops are implemented with 10 dB signal margin to guarantee the stability in case of shocks of the hosting structure, the classical inertial actuator can produce only about 14.4 dB (blue circle) kinetic energy reduction. Instead, the feedback loops with the flywheel inertial actuators can still produce 16.2 dB of the kinetic energy reduction.

5 CONCLUSIONS

This paper has presented experimental tests of the new electro-magnetic actuator equipped with the flywheel element for the implementation of the velocity feedback control loops on thin plate structure. A base impedance study has shown that the inertial actuator is characterised by low and high frequencies mass impedance proportional respectively to the total and the base mass of the actuator. The actuator equipped with the flywheel element presented a similar base impedance spectrum although the amplitude of the resonance peak and antiresonance low were much smaller as the resonance and antiresonance frequencies were moved to lower frequencies and were much closer to each other. The experimental results on the frequency response functions that characterise the electromechanical response showed good correlation to the simulation results.

The stability and control performance of velocity feedback loops implemented on a thin rectangular panel excited by a force point was assessed using the classical inertial actuator and the flywheel configuration. Although all actuators were characterised by the same mass, the flywheel proof mass actuators were characterised by lower fundamental resonance frequency, which compared to the classical inertial actuator was about 6 Hz lower for the flywheel inertial actuator. The stability analysis has shown that the addition of the axial inertia effect produced by the flywheel element increases the gain margin of the velocity feedback loop without increase of the actuator total mass. The stability analysis of the velocity feedback loops implemented on the rectangular plate has shown that the control system with the flywheel inertial actuator has maximum stable signal gain margin equal to 68 dB, which is 13 dB higher compared to the classical inertial actuator.

The 10 Hz - 1 kHz frequency averaged global performance also showed that when the velocity feedback loops were implemented with with 10 dB signal gain margin to prevent the excessive control spillover at the fundamental resonance frequency of the actuators the flywheel inertial actuators produced vibration reductions of about 16.2 dB. The improved performance of the velocity feedback loops was thanks to lower fundamental resonance frequency of the inertial actuator and increased signal gain that can be applied to the inertial actuators. The results show that the velocity feedback loops can provide the best performance with the highest kinetic energy reduction, while at the same time allowing to use the control system with at least 10 dB signal gain margin to guarantee stability in case of shocks of the hosting structure.

ACKNOWLEDGEMENTS

The authors gratefully acknowledge the European Commission for its support of the Marie Skłodowska-Curie program through the ITN ANTARES project (GA 606817). And its support through the Fast Track project (POIR.01.01.01-00-0217/19).

REFERENCES

[1] A. Kras, P. Gardonio, Velocity feedback control with a flywheel proof mass actuator, *Journal of Sound and Vibration* 402 (2017) 31–50.
[2] A. Kras, P. Gardonio, Active vibration control unit with a flywheel inertial actuator, *Journal of Sound and Vibration* 464 (2020).
[3] E. Garcia, C.S. Webb, M.J. Duke, Passive and active control of a complex flexible structure using reaction mass actuators, *Journal of Vibration and Acoustics* 117 (1) (1995) 116–122.
[4] Y. Okada, K. Matsuda, H. Hashitani, Self-sensing active vibration control using moving-coil-type actuator, *Journal of Vibration and Acoustics* 117 (4) (1995) 411–415.
[5] S. Camperi, M. G. Tehrani, S. J. Elliott, Local tuning and power requirements of a multi-input multioutput decentralised velocity feedback with inertial actuators, *Journal of Mechanical Systems and Signal Processing* 117 (2019) 689–708.
[6] C.G. Diaz, C. Paulitsch, P. Gardonio, Smart panel with active damping units. Implementation of decentralized control, *The Journal of the Acoustical Society of America* 124 (2) (2008) 898–910.
[7] S. Camperi, M. G. Tehrani, S. J. Elliott, Parametric study on the optimal tuning of an inertial actuator for vibration control of a plate: Theory and experiments, *Journal of Sound and Vibration* 435 (2018) 1–22.
[8] S.J. Elliott, M. Serrand, P. Gardonio, Feedback stability limits for active isolation systems with reactive and inertial actuators, *Journal of Vibration and Acoustics* 123 (2) (2001) 250–261.
[9] C.G. Diaz, P. Gardonio, Feedback control laws for proof-mass electro-dynamic actuators, *Smart Materials and Structures* 16 (2007) 1766–1783.
[10] D.B. Hiemstra, G. Parmar, S. Awtar, Performance Tradeoffs Posed by Moving Magnet Actuators in Flexure-Based Nanopositioning, *IEEE/ASME Transactions on mechatronics* 1 (19) (2014).
[11] C. Paulitsch, P. Gardonio, S.J. Elliott, P. Sas, R. Boonen, *Design of a lightweight, electrodynamic, inertial actuator with integrated velocity sensor for active vibration control of a thin lightly-damped panel,* Proceedings of the 2004 International Conference on Noise and Vibration Engineering, ISMA, (2005) 239-253.
[12] C. Paulitsch, *Vibration control with electrodynamic actuators,* VDI Verlag, Düsseldorf, 2005.
[13] J. Rohlfing, P. Gardonio, S.J. Elliott, Base impedance of velocity feedback control units with proof-mass electrodynamic actuators, *Journal of Sound and Vibration* 330 (20) (2011) 4661–4675.
[14] M. D. Borgo, M. G. Tehrani, S. J. Elliott, Identification and analysis of nonlinear dynamics of inertial actuators, *Journal of Mechanical Systems and Signal Processing* 115 (2019) 338–360.
[15] O.N. Baumann, S.J. Elliott, Destabilization of velocity feedback controllers with stroke limited inertial actuators, *The Journal of the Acoustical Society of America* 121 (5) (2007) 211–217.
[16] O. N. Baumann, S. J. Elliott, The stability of decentralized multichannel velocity feedback controllers using inertial actuators, *The Journal of the Acoustical Society of America*, 121 (1) (2007) 188–196.
[17] C.G. Diaz, C. Paulitsch, P. Gardonio, Active damping control unit using a small scale proof mass electrodynamic actuator, *The Journal of the Acoustical Society of America* 124 (2) (2008) 886–897.
[18] P. Gardonio, C.G. Diaz, Downscaling of proof mass electro-dynamic actuators for decentralised velocity feedback control on a panel, *Smart Materials and Structures* 19 (2) (2010) 1–14.
[19] N. Alujević, H. Wolf, P. Gardonio, I. Tomac, Stability and performance limits for active vibration isolation using blended velocity feedback, *Journal of Sound and Vibration*, 330 (21) (2011) 4981–4997.
[20] M. Zilletti, Feedback control unit with an inerter proof-mass electrodynamic actuator, *Journal of Sound and Vibration* 369 (2016) 16–28.
[21] N. Alujević, D. Čakmak, H. Wolf, M. Jokić, Passive and active vibration isolation systems using inerter, *Journal of Sound and Vibration*, 418 (2018) 163–183.